Nature Communications

https://doi.org/10.1038/s41467-026-70519-8

Article in Press

Dopamine and serotonin inversely modulate D2 medium spiny neurons to regulate cocaine reward

Received: 5 May 2025

Accepted: 26 February 2026

Cite this article as: Cardozo Pinto, D.F., Guo, M.Y., Pomrenze, M.B. *et al.* Dopamine and serotonin inversely modulate D2 medium spiny neurons to regulate cocaine reward. *Nat Commun* (2026). https://doi.org/10.1038/s41467-026-70519-8

Daniel F. Cardozo Pinto, Michaela Y. Guo, Matthew B. Pomrenze, Wade Morishita, Mona X. Li, Larry S. Zweifel, Neir Eshel & Robert C. Malenka

Dopamine and serotonin inversely modulate D2 medium spiny neurons to regulate cocaine reward

Daniel F. Cardozo Pinto[1,2,3,*,‡], Michaela Y. Guo[1,*], Matthew B. Pomrenze[1], Wade Morishita[1], Mona X. Li[1], Larry S. Zweifel[4,5], Neir Eshel[6,†,‡], and Robert C. Malenka[1,†,‡]

[1] Nancy Pritzker Laboratory, Department of Psychiatry and Behavioral Sciences, Stanford University School of Medicine, Stanford, CA 94305, USA

[2] Current address: Society of Fellows, Harvard University, Cambridge, MA 02138, USA

[3] Current address: Department of Molecular and Cellular Biology, Harvard University, Cambridge, MA 02138, USA

[4] Department of Psychiatry and Behavioral Sciences, University of Washington, Seattle, WA 98195, USA

[5] Department of Pharmacology, University of Washington, Seattle, WA 98195, USA

[6] Department of Psychiatry and Behavioral Sciences, Stanford University School of Medicine, Stanford, CA 94305, USA

* These authors contributed equally

† These authors jointly supervised this work

‡ Correspondence: dcardozopinto@fas.harvard.edu

neshel@stanford.edu

malenka@stanford.edu

ABSTRACT

Classic theories propose opponent functions for striatal dopamine (DA) and serotonin (5-hydroxytryptamine; 5HT), with DA promoting approach and 5HT promoting patience or avoidance. How these neuromodulators regulate downstream circuits to achieve such antagonistic effects remains mysterious. Here, we mapped striatal 5HT receptor expression in mice to reveal preferential enrichment of putatively excitatory, G_q-coupled 5HT receptors on medium spiny neurons expressing inhibitory D2 DA receptors (D2-MSNs). Acute slice recordings from genetically identified striatal neurons showed that DA and 5HT inversely regulate D2-MSN firing and confirmed that 5HT's excitatory effect on these cells is blocked by 5HT2a and 5HT2c receptor antagonists. Pharmacologically upregulating striatal 5HT release preferentially induced cfos expression in D2-MSNs, validating that 5HT's excitatory effect on these cells also occurs *in vivo*. Finally, 5HT2c receptor loss-of-function in D2-MSNs, but not D1-MSNs, enhanced animals' sensitivity to the behavioral effects of cocaine – a potent releaser of DA and 5HT – showing that 5HTergic excitation of D2-MSNs counteracts the reinforcing effects of striatal DA release. Altogether these results demonstrate that DA and 5HT inversely modulate D2-MSN activity to regulate cocaine reward, identifying a key circuit mechanism underlying the opponent behavioral effects of these important neuromodulators.

INTRODUCTION

Striatal DA release is crucial for animals to learn from and seek rewards[1]. Longstanding theories have proposed that 5HT works against DA by promoting behavioral suppression or driving aversive learning[2–7]. These influential notions of opponency are supported by pharmacology experiments showing that 5HT-releasing drugs blunt the DA-driven rewarding effects of drugs of abuse[8–11], as well as by studies showing that 5HT activity can suppress reward-seeking behavior[12–16]. Consistent with an oppositional relationship between striatal DA and 5HT, we recently found that rewards trigger opposite striatal DA and 5HT responses and that both of these inverse signals are required for a stimulus to be maximally reinforcing[17]. However, it remains unclear how opponent DA and 5HT signals regulate striatal activity to exert opposing effects on behavior.

In the striatum, DA works at least in part by differentially modulating excitability and plasticity in two primary projection neuron classes. DA is thought to increase activity in medium spiny neurons expressing the G_s-coupled D1 DA receptor (D1-MSNs) and decrease activity in those expressing the G_i-coupled D2 receptor (D2-MSNs)[18,19]. In contrast, there is much more limited understanding of the effects of 5HT on striatal circuits. Owing to the limited spatial and

cell-type resolution of transcriptomic[20] and autoradiographic[21] studies, respectively, how 5HT receptors are organized across striatal subregions and cell-types remains unclear. As a result, the mechanisms by which 5HT may modulate striatal physiology to counteract DA's behavioral effects are poorly understood. Here, we map striatal 5HT receptor expression to reveal that putatively excitatory 5HT receptors are enriched on D2-MSNs and show that 5HTergic excitation counteracts striatal DA's inhibitory effect on their activity in a manner that constrains the reinforcing properties of cocaine.

RESULTS

First, we set out to identify which 5HT receptors are expressed on MSNs by mining a single-cell RNA-sequencing dataset of the mouse striatum[22]. We found that the vast majority (>90%) of MSNs express 5HT receptors, including members of the G_i-, G_s-, and G_q- coupled 5HT receptor families but not the ionotropic receptor 5HTR3 (**Supplementary Fig. 1a-c**). Of the 14 5HT receptor genes found in mice, 7 are widely expressed in MSNs (*Htr1b*, *Htr1d*, *Htr1f*, *Htr2a*, *Htr2c*, *Htr4*, *Htr6;* **Supplementary Fig. 1d,e**), and one more is known to be expressed in a unique minority MSN population in rodents[22,23] and humans[24] (*Htr7*). Some 5HT receptor genes showed differential expression between striatal patch and matrix compartments and many were correlated with expression of D1- or D2- MSN marker genes (**Supplementary Fig. 1f,g)**. Together, these results suggest that 5HT receptor expression in striatal MSNs is nearly ubiquitous, restricted primarily to 8 receptor genes, and varied across cell-types and subregions.

To better understand striatal 5HT receptor organization, we next used fluorescence *in situ* hybridization to map expression of the subset of genes identified above. In each experiment, we labeled transcripts for the D1 receptor *(Drd1a*), the D2 receptor (*Drd2*), and one 5HT receptor gene, allowing us to identify putative D1- and D2- MSNs (pD1- and pD2-MSNs, respectively) and measure spatial location and receptor expression individually for each cell. Control samples labeled for the MSN marker gene *Ppp1r1b* validated that this approach accurately identifies MSNs which could be divided into pD1 and pD2 subpopulations based on their DA receptor expression profiles (see Methods and **Supplementary Fig. 2a-e**).

Expression of every 5HT receptor gene that we examined varied across cell-types and subregions (**Fig. 1a-h**). At the cell-type level, pD1- and pD2- MSNs both expressed G_i-, G_s-, and G_q- coupled 5HT receptors but showed quantitative differences in expression of individual receptor genes (**Supplementary Fig. 3a-d**). pD1-MSNs were preferentially enriched for G_i-coupled *Htr1f* and G_s-coupled *Htr4* receptors which co-labeling experiments showed to be widely co-expressed in individual neurons, suggesting 5HT may have a relatively balanced net

effect on the activity of these cells (**Fig. 1 c,f** and **Supplementary Fig. 4a-c**). By contrast, pD2-MSNs were most strongly enriched for the G_s-coupled *Htr7* and G_q-coupled *Htr2a* and *Htr2c* receptors, suggesting that 5HT may have a net excitatory effect on the activity of these cells (**Fig. 1d,e,h** and **Supplementary Fig. 4d-f**). Spatially, individual 5HT receptor genes were preferentially expressed in dorsal (*Htr7:* DMS, DLS), ventral (*Htr1f*: NAc^{medSh}, NAc^{core}, NAc^{latSh}; *Htr4:* NAc^{medSh}, NAc^{latSh}), medial (*Htr2c:* NAc^{medSh}, NAc^{core}), or lateral (*Htr2a:* NAc^{latSh}) striatal subregions, and some were enriched (*Htr2a*, *Htr7*) or depleted (*Htr1b*) in irregular patchy patterns consistent with striosome and matrix organization, respectively (**Fig. 1i**).

This spatial heterogeneity in 5HT receptor gene expression raised the question of which striatal subregions receive the most 5HT input. By analyzing labeled axons from dorsal raphe 5HT (DR^{5HT}) neurons[17] – the primary source of striatal 5HT input[25] – we found that 5HT inputs were denser in the nucleus accumbens (NAc) compared to the dorsal striatum (consistent with reports in rats[26–28] and primates[29,30]; **Supplementary Fig. 5a,b**), and densest in the posterior NAc medial shell (NAc^{medSh}; **Fig. 1j** and **Supplementary Fig. 5c-g**). Examining cell-type differences in 5HT receptor expression in this region further suggested that striatal pD1- and pD2-MSNs may be differentially regulated by 5HT, likely in a manner approximately opposite to their modulation by DA (**Fig. 1k**).

To test this hypothesis, we performed acute slice recordings from genetically identified D1- and D2- MSNs in the NAc^{medSh} and measured their responses to bath application of DA or 5HT (**Fig. 2a**). We did this in cell-attached mode to prevent dialyzing the cell – which interferes with the intracellular signal transduction cascades recruited by G-protein coupled receptors[31,32]– and in the presence of potassium channel blockers to induce spontaneous activity in normally quiescent MSNs, allowing us to detect both increases and decreases in MSN activity in response to DA or 5HT (**Fig. 2b,c**). In agreement with previous work[18,19,32], we found that DA increased activity of D1-MSNs and decreased activity of D2-MSNs (**Fig. 2d-g** and **Supplementary Fig. 6a,b**). By contrast, bath application of 5HT did not significantly change D1-MSN activity, but it excited D2-MSNs (**Fig. 2h-k** and **Supplementary Fig. 6c,d**). This was consistent with these cell-types' distinct 5HT receptor expression profiles and indicated that DA and 5HT differentially regulate the activity of the two primary striatal cell-types (**Fig. 2l-m**). In subsequent experiments, application of 5HT2a and 5HT2c receptor antagonists was sufficient to completely abolish 5HT's excitatory effect on D2-MSNs, confirming that this effect is mediated by G_q-coupled 5HT2-family receptors (**Fig. 2 n-o**).

To examine whether the excitatory effect of 5HT on D2-MSNs observed in slice also occurs *in vivo*, we implanted *Drd1a-TdTomato;Drd2-eGFP* double reporter mice with drug

infusion cannulas above the NAc^{medSh}, locally infused saline or the 5HT reuptake inhibitor escitalopram to enhance striatal 5HT signaling, and immunostained for the immediate early gene product cfos as a proxy for neural activity (**Fig. 2p**). While escitalopram-treated mice showed similar total numbers of cfos+ MSNs compared to saline-treated controls, cfos expression was preferentially localized to D1-MSNs in the saline-treated group and to D2-MSNs in the escitalopram-treated group, suggesting that 5HT also has an excitatory effect on D2-MSNs *in vivo* (**Fig. 2q-t** and **Supplementary Fig. 7a**). Importantly, this effect was unlikely to be explained by off-target effects of our pharmacological manipulations, as fiber photometry recordings with genetically encoded sensors for DA and 5HT confirmed that escitalopram robustly enhances striatal 5HT release with only modest effects on striatal DA (**Supplementary Fig. 7b-c**). Altogether, our electrophysiological recordings and cfos data suggest that 5HT generally counteracts DA's effects on striatal physiology, and this effect is especially pronounced in D2-MSNs where excitatory, Gq-coupled 5HT receptors directly oppose DA's inhibitory effect on these cells in slice and *in vivo*.

In a final set of experiments, we sought to test whether 5HT's effects on striatal activity functionally oppose the behavioral effects of striatal DA signaling. We reasoned that if DA release drives reinforcement at least in part by inhibiting D2-MSNs, then 5HTergic excitation of the same neurons should constrain the rewarding properties of a stimulus that evokes release of both neuromodulators, such as cocaine. To test this hypothesis, we injected Drd1-Cre and Adora2a-Cre mice in the NAc^{medSh} with bicistronic viral vectors encoding the Cas9 endonuclease from *Staphylococcus aureus* (SaCas9)[33] and single-guide RNAs for *Htr2c* or the control locus *Rosa26* (**Fig. 3a**). In this way, we induced loss-of-function mutations of *Htr2c* – the most highly expressed G_q-coupled 5HT receptor in the NAc^{medSh} — in either D1- or D2- MSNs with cell-type specificity.

We then tested these mice on a subthreshold cocaine conditioned place preference (CPP) paradigm (**Fig. 3b**). We chose cocaine for this experiment because it evokes robust increases in striatal DA and 5HT[34,35] and used a modest dose (5mg/kg) to enable us to detect increases in the CPP score without the confound of ceiling effects. Furthermore, cocaine reward related behaviors have been shown to require striatal DA release[36,37], to be enhanced by D1-MSN activation[38,39], and to be suppressed by D2-MSN activation[38–40]; making cocaine CPP a powerful assay to study how DA and 5HT regulate striatal circuits to control reward and reinforcement. We found that mice with *Htr2c* loss-of-function in D1-MSNs showed no difference in their locomotor or CPP responses to cocaine compared to *Rosa26* controls (D1-sgHtr2c and D1-sgRosa, respectively; **Fig. 3c-f**). By contrast, mice with *Htr2c* loss-of-function in D2-MSNs

showed a trend toward increased locomotor sensitization and exhibited an enhanced place preference for cocaine compared to *Rosa26* controls (D2-sgHtr2c and D2-sgRosa, respectively; **Fig. 3g-j**). Importantly, these effects could not be explained by changes in general locomotion induced by our manipulations because neither the D1-sgHtr2c nor the D2-sgHtr2c group showed any detectable changes in locomotor behavior at baseline (**Supplementary Fig. 8a**). Additionally, the behavior of mice in the D1- and D2- sgRosa control groups was identical, further arguing against the possibility that off-target effects from our genetic manipulations could contribute to the behavioral changes observed in the D2-sgHtr2c group (**Supplementary Fig. 8b-e**). Instead, *Htr2c* loss-of-function in D2-MSNs, but not D1-MSNs, appeared to specifically enhance animals' sensitivity to the behavioral effects of striatal DA release induced by cocaine (**Fig. 3k-l**). Consistent with this interpretation, behavioral measures of cocaine's locomotor, sensitizing, and rewarding effects were significantly correlated for mice in the D2-sgHtr2c group but not for the D1-sgHtr2c or control groups (**Fig. 3m-n**). Altogether, these results suggest that 5HT2c receptor-mediated excitation of D2-MSNs constrains the DA-dependent reinforcing effects of cocaine, showing that 5HTergic modulation of striatal physiology functionally opposes the behavioral functions of striatal DA release.

DISCUSSION

Here we built a molecular map of striatal 5HT receptor expression, found that G_q-coupled 5HT2-family receptors are enriched on D2-MSNs, showed that 5HT has an excitatory effect on these cells, and demonstrated that 5HT counteracts DA's effects on striatal physiology and behavioral reinforcement. Collectively, our results identify inverse regulation of D2-MSN activity by DA and 5HT as a key mechanism underlying opponent control of reinforcement by striatal DA and 5HT[17] and suggest that this opponency regulates learning for drugs as well as natural rewards. Thus, our work provides a circuit-level explanation for longstanding observations of antagonistic behavioral effects driven by DA and 5HT.

Our results are consistent with previous electrophysiology studies showing that activation of 5HT2-family receptors can depolarize some striatal neurons via reduction of potassium currents[41,42]. These results also agree with observations of 5HT2a or 5HT2c receptor activation dampening the rewarding effects of cocaine[10,43–47] as well as with reports of increased sensitivity to cocaine following manipulations that blunt cocaine-evoked 5HT release[48,49] or inactivate receptors in the 5HT2 family[11,50]. Given that the manipulations in these studies lacked spatial and/or cell-type specificity, our study builds on these findings by identifying striatal D2-MSNs as a primary locus of action for these physiological and behavioral effects. Notably,

numerous studies report that 5HT release and/or agonism of 5HT2 receptors also reduce reinforcement, sensitization, or seeking for nicotine[51], ethanol[52,53], amphetamines[8,9], MDMA[54] (3,4-methylenedioxymeth-amphetamine; “ecstasy”), and opioids[53,55,56]. This suggests that the circuit motif we describe by which 5HT reduces the rewarding effects of DA is not specific to cocaine but may represent a general mechanism by which striatal 5HT signaling exerts a protective effect against reinforcement for a wide variety of psychoactive substances with addictive liability and/or useful clinical applications.

These data are particularly interesting in view of renewed interest in the potential of psychedelics – which act as agonists at the 5HT2a and 5HT2c receptors, among others – to treat substance abuse disorder[57–59]. A major goal in this branch of work is to design or identify compounds that retain potentially therapeutic properties of psychedelics without the hallucinogenic effects[53]. Although the precise neural mechanisms that underlie hallucinogenesis are still unknown, the prevailing view is that 5HT2a receptors in the cortex play a central role in this process[60,61]. In this context, our results suggest that targeting 5HT2c receptors (as opposed to 5HT2a) and/or 5HT2-family receptors in the striatum (as opposed to the cortex) may prove to be fruitful strategies in the development of novel and effective treatments for substance abuse disorder with reduced potential for hallucinogenic side effects.

More broadly, our work elucidating the distribution of 5HT inputs and receptors in the striatum opens important research avenues into how striatal DA and 5HT modulate striatal physiology to shape a wider range of motivated behaviors. In other behavioral contexts, the opponent regulation of striatal output pathways by DA and 5HT may be complemented by additional actions reported for these neuromodulators in the striatum, which include modulating the strength of corticostriatal[62–64] and thalamostriatal[65,66] synapses, differentially filtering presynaptic inputs onto MSNs[66], and regulating lateral inhibition between D1 and D2 MSNs[67–69]. Notably, a growing body of work suggests that DA and 5HT may inversely regulate some cholinergic interneurons –which express inhibitory D2 DA receptors and excitatory 5HT2-family receptors for 5HT– while exerting heterogeneous effects on various subtypes of GABAergic interneurons[70–77]. We anticipate that identifying how each of these mechanisms contributes to behavioral functions ascribed to striatal DA and 5HT beyond reinforcement – including decision making[78,79], sociability[80–82], and aggression[83–85] – will be an important future direction for the field.

METHODS

Mice

C57BL6/J (Jackson Laboratory #000664), *Drd1a-TdTomato* (Jackson Laboratory #016204), *Drd2-eGFP* (Jackson Laboratory #030255), *Drd1a-TdTomato;Drd2-eGFP* (cross between Jackson Laboratory #016204 and #030255), *Drd1-Cre (*MMRRC #029178-UCD*)*, and *Adora2a-Cre* (MMRRC #036158-UCD), and *SERT-Cre* (MMMRC #017260-UCD) mice of both sexes (>5 weeks old) were used in this study. Mice were housed at ~21°C with 30-70% humidity on a 12-hour light/dark cycle with ad-libitum access to food and water. All experimental procedures were approved by the Stanford University Administrative Panel on Laboratory Animal Care and the Administrative Panel on Biosafety.

Stereotactic surgeries

Stereotactic surgeries were performed as previously described[17]. Mice were anesthetized with isoflurane (4-5% induction, 1-2% maintenance) and a stereotaxic frame (Kopf instruments) was used to target injections and implantations to the following structures (coordinates are in mm, with AP and ML relative to bregma and DV relative to the skull surface): DR, AP -4.6, ML 0, DV -3.3; NAc^{medSh}, AP +1.0, ML +/-0.7, DV -4.3. Viral vectors (diluted to between 10^{12} and 10^{13} gc/ml, except for photometry viruses which were used at stock titer) were infused with a syringe pump (Harvard Apparatus) at a rate of 100-200 nL/min and allowed to diffuse for at least 5 min. Drug infusion guide cannulas and/or fiber optic cannulas were secured to the skull using screws (Antrin Miniature Specialties) and dental cement (Geristore). Viral incubation times were >3 weeks. Drug infusion guide cannulas placements were histologically verified post-hoc.

Fluorescence *in situ* hybridization mapping of 5HT receptor expression

Fluorescence in situ hybridization was performed as previously described[86]. Briefly, wild-type mice were deeply anesthetized with isofluorane and then decapitated. The brains were dissected and flash frozen in isopentane on dry ice. Coronal sections of the striatum (16 um thick, approximately from 0.74 to 1.70 mm anterior to bregma) were collected on a cryostat, and samples were prepared following the RNAscope Multiplex Fluorescent Reagent Kit v2 protocol from ACDBio, using 1 hr on ice cold PFA for fixation and 5 min treatment with Protease Plus for digestion. The following probes were used, all from ACDBio: *Drd1a* (#406491, #406491-C2), *Drd2* (#406501-C3), *Htr1b* (#315861-C2), *Htr1d* (#315871-C2), *Htr1f* (#315881-C2), *Htr2a* (#401291-C2), *Htr2c* (#401001-C2), *Htr4* (#408241), *Htr6* (#411161), *Htr7* (#401321-C2), and

Ppp1r1b (#405901-C2). The *Drd1a* and *Drd2* probes were used for all experiments, while the third labeled gene varied across different experiments, and slides were coverslipped with Fluoromount-G containing DAPI (Southern Biotech, 0100-20). Thus, all samples were labeled for DAPI, *Drd1a*, *Drd2*, and one more gene that varied across experiments (either a 5HT receptor gene or the MSN marker gene *Ppp1r1b*).

Stitched images of the entire striatum in each hemisphere were acquired on a Keyence BZ-X800 microscope running BZ-X800 Viewer software using a 10x, 0.45 NA objective with a resolution of ~0.755 um/pixel. Exposure times for the DAPI, *Drd1a*, and *Drd2* channels was kept constant across all experiments. Owing to differences in the expression level of the various 5HT receptor genes and the MSN marker gene *Ppp1r1b*, exposure times for imaging the third channel varied across experiments, but within an experiment all samples were imaged with identical settings and quantifications presented show only relative, not absolute, differences to account for the different exposure times used. Subsequent image analysis was carried out in ImageJ to perform cell-detection based on the DAPI channel and then measure signal in the other fluorescent channels separately for each detected cell. Specifically, each fluorescent channel was preprocessed as follows. DAPI channel: background subtraction (rolling ball, radius 50 pixels), top-hat filter (radius 12 pixels), Mexican hat filter (radius 7 pixels). *Drd1a* and *Drd2* channels: background subtraction (rolling ball, radius 50 pixels), top-hat filter (radius 12 pixels). 5HT receptor gene or *Ppp1r1b* channel: background subtraction (rolling ball, radius 50 pixels). All preprocessed channels were then duplicated and one copy of each channel was binarized as follows: DAPI, thresholding using Li's algorithm[87], opening, watershedding, and opening; *Drd1a* and *Drd2* channels, thresholding using Li's algorithm[87], erosion; 5HT receptor gene and *Ppp1r1b* channel, thresholding (using the moments algorithm[88] for 5HT receptor experiments and Otsu's algorithm for *Ppp1r1b* experiments, followed by a dilation operation for *Ppp1r1b*-labeled samples only). Samples were then manually annotated for striatal subregions based on DAPI signal and the Paxinos brain atlas[89] (excluding the Islands of Calleja), and cell-detection was done by applying the ImageJ Analyze Particles function (size = 64-324, circularity = 0.25-1.00) to the binarized DAPI channel. Cell-ROIs were then overlayed onto the preprocessed and binarized fluorescence channels to measure the mean brightness and percentage of area covered by fluorescence signal in each channel for each cell, and the coordinates and striatal subregion of each detected cell were also recorded.

Putative D1 and D2 MSNs were then identified on the basis of their *Drd1a* and *Drd2* signals. First, cells with low DA receptor expression (defined as <75% area covered by *Drd1a* or *Drd2* signal) were excluded. Then, a cell-type identity index was calculated as ([*Drd1a* area

covered – *Drd2* area covered] / [*Drd1a* area covered + *Drd2* area covered]) for each cell. Cells with a score less than 0 were assigned the pD2-MSN label and cells with a score greater than 0 were assigned the pD1-MSN label. A very small minority of cells with a cell-type identity score equal to 0 (i.e. equal amounts of *Drd1a* and *Drd2* signal) were excluded from further analysis (see Supplementary Fig. 2e). These image preprocessing steps and the chosen cutoff values were validated using a dataset where the MSN marker gene *Ppp1r1b* was labeled instead of a 5HT receptor gene, as shown in Supplementary Fig 2. This control experiment confirmed that the image analysis pipeline described above accurately identified MSNs and the resulting population of cells showed a clear bimodal distribution of *Drd1a* and *Drd2* expression enabling us to assign pD1- and pD2- MSN identities accordingly.

After pD1- and pD2- MSNs were identified as described above, 5HT receptor expression was compared across striatal subregions and cell-types as follows. 5HT receptor expression reconstruction maps in Fig 1 were generated by selecting an example hemisphere for each experiment and plotting each pMSN in that hemisphere as a dot at its corresponding coordinates in the original image. Each dot was then colored by cell-type and scaled in size and opacity by the signal in the 5HT receptor channel for that cell (percentage of each cell's area covered by 5HT receptor gene signal, scaled separately for each 5HT receptor gene using the scale function in R with center=FALSE and scale=TRUE). The relative expression bar graphs in Fig 1 show the percentage of each cell's area covered by 5HT receptor gene signal averaged within each cell-type and subregion for each mouse and normalized to the highest expressing cell-type and subregion for that gene. Finally, the cell-type preference index graphs in Fig 1k and Supplementary Fig. 3 were generated by averaging the percentage of area covered by 5HT receptor signal across cells for each mouse within cell-types and subregions, and then calculating a cell-type preference index for each receptor with the formula ([average 5HTR area covered in pD1 cells - average 5HTR area covered in pD2 cells]/[average 5HTR area covered in pD1 cells + average 5HTR area covered in pD2 cells]).

Fluorescence *in situ* hybridization mapping of 5HT receptor co-expression

Fluorescence in situ hybridization was performed as described above except that samples were co-labeled with probes from ACDBio for the *Drd1a* (#406491), *Htr1f* (#315881-C2), and *Htr4* (#408241-C3) transcripts or the Drd2 (#406501), *Htr2a* (#401291-C2), *Htr2c* (#401001-C3) transcripts to evaluate co-expression of 5HT receptors enriched on D1- and D2-MSNs, respectively. Image acquisition and processing were done as described above, except that the preprocessing for the DAPI channel used a sharpening and top-hat filter (radius 7 pixels)

operation in lieu of the Mexican hat filter. Cells that met DA receptor expression criteria were identified as pD1- and pD2- MSNs (>75% cell area covered by thresholded *Drd1a* and *Drd2* signal, respectively) and the brightness and fraction of area covered by signal in the 5HT receptor gene channels were measured for each of those cells.

RNAseq analysis

RNAseq data shown in Supplementary Fig 1a-g originated from Stanley et al[22]. We performed original analyses on this data beginning with the count matrix, which listed the number of reads detected of each gene for every cell that met the original paper's quality control standards, and the metadata matrix which contained the discrete and continuous cell-type identities assigned to each cell in the count matrix. Cells from the olfactory tubercle and islands of Calleja (continuous subtypes "OT.ruffle", "OT.flat", and "ICj") were excluded from analysis and 5HT receptor genes that were not detected in any cell in the dataset were assigned a count value of 0 (*Htr3a*, *Htr3b*). For the remaining data, the expression level (as counts per million reads; cpm) and fraction of cells (as a percentage) expressing at least one read was calculated for each 5HT receptor gene and averaged within mice. For the patch vs matrix comparison, the same calculation was done separately for cells that were assigned patch or matrix sub-type identities in the original Stanley et al [22] paper on the basis of their gene expression profiles (patch: continuous subtypes "Htr7.vMedPat", "Pat.Dorsolateral_CPu", "Pat.Ventromedial_CPu"; matrix: continuous subtypes ""Mat.Dorsolateral_CPu", "Mat.Ventromedial_CPu"). See Stanley et al.[22] Methods for additional details on RNAseq data preprocessing and patch/matrix cell-type identity assignments. Finally, gene expression correlation analysis was done by calculating the Spearman correlation between scaled log expression levels for D1 and D2 marker genes and 5HT receptor genes for all cells pooled across mice.

Histology and Immunohistochemistry

Histology and immunohistochemistry were performed as previously described[17]. Mice were transcardially perfused with 4% (w/v) paraformaldehyde (PFA) in phosphate-buffered saline (PBS), and the brains were postfixed in PFA overnight before being sectioned coronally to a thickness of 50 um on a vibratome. Sections were then washed three times for 10 min in PBS, blocked and permeabilized for 1 hr in a solution of 10% normal goat serum, 0.2% bovine serum albumin, and 0.5% triton-X, washed once for 5 min in PBS, incubated with primary antibodies in carrier solution (1% normal goat serum, 0.2% bovine serum albumin, and 0.5% triton-X) overnight on a shaker at room temperature, washed four times for 10 min, incubated for 2 hr

with secondary antibodies in carrier solution, and finally washed four times for 10 min in PBS before being mounted on microscope slides and coverslipped with Fluoromount-G containing DAPI (Southern Biotech #0100-20). For axon tracing experiments, sections were immunostained for EYFP (primary: chicken anti-GFP, Aves #GFP-1020; secondary: goat anti-chicken 488, Invitrogen #A-11039) and/or mCherry (primary: rat anti-mCherry, Invitrogen #M11217; secondary: goat anti-rat 594, Invitrogen #11007). For immediate early gene experiments, sections were immunostained for cfos (primary: rabbit anti-cfos, Sysy #226008; secondary: goat anti-rabbit 647, Invitrogen # A-21244). Primary antibodies were used at a concentration of 1:1000 and secondary antibodies were used at a concentration of 1:750.

Axon tracing

The axon tracing data presented in Supplementary Fig. 5a-e are a new analysis of data that were collected and published previously[17]. For the DR^{5HT} presynaptic bouton labeling experiments in Supplementary Fig. 5f-g, SERT-Cre mice were injected in the DR with 1 uL of AAV-DJ-hSyn-GFP-2A-synaptophysin-mRuby, immunostained for EYFP and mCherry, and example images were captured on a Nikon A1 confocal microscope.

Intra-NAc drug infusions and cfos screen

Intra-NAc drug infusion experiments were performed on *Drd1a-TdTomato;Drd2-eGFP* double transgenic mice. Guide cannulas (Protech International) were surgically implanted unilaterally 1 mm above the NAc^{pmSh} (i.e. -3.3 mm DV) such that the tip of the infusion cannula (Protech International), which protruded 1 mm past the tip of the guide cannula, would reach the target coordinate on the day of the experiment. After recovery from surgery (>1 week), mice received 1-2 days of habituation to handling, to the open field behavioral arena, and to being tethered, and one sham intra-NAc infusion of saline. On the day of the experiment, the infusion cannula was attached via tubing to a 5 uL syringe (Hamilton) mounted on a syringe pump (Harvard apparatus) and threaded through the guide cannula to reach the target structure in each mouse. Mice then received either 500 nL saline or 2.5 ug of escitalopram oxalate (Tocris) dissolved in 500 nL of saline infused at a rate of 150 nL/min. Mice were allowed to recover for 5-10 min in the home cage after the infusion completed before being placed into the open field arena for 90 min and then were immediately perfused. The brains were processed for cfos immunohistochemistry as described above and imaged as follows. For each of 6-8 sections per mouse, we acquired one image of the NAc^{medSh} (AP +0.98-1.34 mm from bregma) on the implanted hemisphere (~300 um x ~300 um, 40x 1.3 NA objective, Nikon A1 confocal

microscope running NIS Elements AR 5.02.00 software). The TdTomato, eGFP, and cfos channels of these images were then processed in ImageJ as follows: top hat filter (100 px radius), background subtraction (rolling ball radius 50 px), and thresholding with the moments algorithm [88]. TdTomato+/cfos+ and eGFP+/cfos+ cells were then manually counted.

Slice electrophysiology

Coronal striatal slices were prepared as previously described[86]. *Drd1a-tdTomato* or *Drd2-eGFP* mice (P60-90) were decapitated following deep isoflurane anesthesia. The brain was quickly removed and placed in ice cold cutting solution (bubbled with 95%O2/5%CO2) consisting (in mM): 228 sucrose, 2.5 KCl, 1.0 NaH2PO4, 8 MgSO4, 26 NaHCO3, 20 glucose and 0.5 CaCl2. The forebrain was isolated, mounted on a cutting platform, and hemisected prior to slicing. Coronal slices (200 µm thick) containing the NAc were cut with a vibratome (Leica VT1000s) and transferred to a holding chamber containing warmed (30 C, bubbled with 95%O2/5%CO2) ASCF consisting (in mM): 119 NaCl. 2.5 KCl, 1 NaH2PO4, 1.3 MgCl2, 26 NaHCO3, 10 glucose and 2.5 CaCl2. Slices were incubated for 45 min and then kept at room temperature for 1-1.5 hrs before being transferred to the fixed recording chamber of an upright microscope (BX50WI, Olympus). Slices were perfused with ACSF (bubbled with 95%O2/5%CO2) and maintained at 30-32 C. D1- and D2- MSNs in the medial shell of posterior NAc slices were identified by epifluorescence. To prevent dialysis of intracellular contents, which can interfere with G-protein signaling cascades of interest in this study, cell-attached voltage-clamp recordings were made using patch electrodes containing (in mM): 146 NaCl, 10 HEPES (pH adjusted to 7.4 with NaOH)[90]. Electrode resistances ranged from 6-8 MΩ. Cell-attached recordings were maintained at a holding potential of -10 mV and resistances (> 1 GΩ) were continually monitored by delivering a 4 mV, 100ms voltage-pulse every 20 s. Cell-attached voltage-clamp recordings were acquired with a MultiClamp 700B (Molecular Devices) and recorded in gap free mode (PClamp 10, Molecular Devices). Signals were filtered at 2 KHz and digitized at 10 KHz (National Instruments BNC-2090 or Digidata 1320A, Axon Instruments). All drugs (Sigma Aldrich) were bath applied and diluted to their final concentrations from concentrated stocks (1000-2000x in dH20). Spontaneous action potentials (APs) were generated by addition of barium chloride (Ba^{2+}, 0.5 mM) and 4-aminopyridine (4-AP, 0.15 mM) to the ACSF. Once steady AP firing had been achieved (~5 min) slices were exposed to either serotonin (5-HT, 25 µM) or dopamine (DA, 100 µM) for 4 min. Effects on AP frequency were quantified in a 3 min window before and the last 3 min of drug exposure. Excitability difference and excitability ratio measures were calculated by taking the difference and the ratio, respectively, of the AP frequencies

measured during these time windows for each cell. In a subset of experiments evaluating the contribution of 5HT2a and 5HT2c receptors to the excitatory effects of 5HT on D2-MSNs, the 5HT2a antagonist MDL100907 (0.1 µM) and the 5HT2c antagonist SB242084 (0.1 µM) were included in the ACSF. APs were analyzed with MiniAnalysis software (Synaptosoft).

Photometry recordings with genetically encoded DA and 5HT sensors

Wildtype mice were injected with 800 nL of a 1:1 cocktail of AAV9-hSyn-GRABrDA2m and AAV9-hSyn-GRAB5HT3.0 viruses from WZBiosciences and implanted with fiber optic cannulas unilaterally above the NAc^{medSh}. After waiting >3 weeks for viral expression, mice were habituated to handling, to the behavioral arena, to being tethered, and to intraperitoneal (i.p.) injections for at least one day. On the day of the experiment, mice were placed into the behavioral arena, connected to optical patch cords and allowed to habituate for at least 3 minutes before we performed fiber photometry recordings. These consisted of a 10 minute baseline period followed by an i.p. injection of 50 mg/kg escitalopram oxalate (Tocris), after which the fiber photometry recording continued for at least 25 more minutes. Data shown correspond to a 30 minute window beginning 5 minutes before the i.p. injection.

Fiber photometry recordings were performed as previously described[17,54]. Briefly, GRAB sensors were excited by 465 nm and 560 nm frequency-modulated light and fluorescence signals were collected through low-autofluorescence patch cords, filtered through a fluorescence minicube, (Doric FMC6_IE(400-410)_E1(460-490)_F1(500-540)_E2(555-570)_F2(590-680)), measured with dedicated photodetectors for each channel (Newport, 2151), sampled at 1.1073 Khz, and demodulated with an Rz5P signal processor running Synapse software (Tucker-Davis Technologies)[17]. Data from each channel underwent preprocessing as follows: the data were de-bleached by fitting a mono-exponential decay function to the 10-minute pre-drug baseline period and subtracting it from the full recording trace, then the mean of the baseline period was used to calculate dF/F using the formula $(F-F_{mean}) / F_{mean}$, and the resulting data were filtered using the filtfilt function with an equally weighted 100 sample window[54]. In post processing, the data were smoothened using a rolling average over a window of 1000 samples, decimated by a factor of 20, and averaged across mice.

Conditioned place preference

To determine if 5-HT2c receptors in the NAc^{medSh} influence the positive reinforcing effects of cocaine, we bilaterally injected Drd1-Cre or Adora2a-Cre mice in the NAc^{medSh} with Cre-dependent CRISPR constructs targeting Htr2c or the control locus Rosa26 (500 nL per

hemisphere of a 1:3 cocktail of AAV-FLEX-eGFP-KASH [addgene #154373] and AAV-FLEX-saCas9-U6-sgHtr2c [addgene # 249541] or AAV-FLEX-saCas9-U6-sgRosa26 [addgene #159914]; all produced by the Zweifel lab at University of Washington, Seattle). The guide sequences for these constructs are the following: sgHtr2c, GGTGTGACCTCGAAGTAACAT; sgRosa26, CTCGATGGAAAATACTCCGAG). After 6-8 weeks of expression, mice were allowed to explore a 2-sided CPP chamber with distinct tactile floors and wall patterns (Med Associates Inc.) in a 15 min pretest. The next morning, mice were confined to one side of the chamber for 15 min after receiving an injection of saline. Approximately 4 hrs later, mice were confined to the opposite side of the chamber immediately after receiving an injection of subthreshold cocaine HCl (5 mg/kg, i.p., Sigma-Aldrich), again for 15 min. This procedure was repeated over the next 2 days for a total of 3 conditioning sessions on each of the saline and cocaine paired sides. Locomotor activity (i.e., distance traveled) was recorded during each of the conditioning sessions. On the 5th day, mice were allowed to explore both sides of the CPP chamber in a 15 min posttest. Preference was calculated as the percentage of time spent in the cocaine-paired side of the chamber during the posttest. CPP was also measured by calculating time spent on the cocaine-paired side during the posttest (cocaine time - saline time) and as a difference score (posttest cocaine time - pretest cocaine time). Cocaine-paired sides were assigned in a counterbalanced and unbiased fashion such that the average preference for the cocaine-paired side during the pretest was ~50% for all groups.

Statistics and reproducibility

Statistical analyses were done in Graphpad Prism and R. Data that met assumptions of normality and equal variance (assessed by inspection of the fitted-values vs residuals and/or Q-Q plots) were analyzed using parametric tests, with two-way ANOVAs followed by Holm-Sidak or Bonferroni post-hoc tests for two-factor designs and t-tests or one-way ANOVAs followed by Holm-Sidak post-hoc tests for one factor designs. Paired or repeated measures and the Greenhouse-Geisser correction were used where appropriate. Data that did not meet assumptions of normality and equal variance underwent the Box-Cox transformation and parametric tests were then used on the transformed data, or the data were analyzed with nonparametric tests instead (Wilcoxon signed-rank test, Friedman test followed by Dunn's multiple comparisons tests). All hypothesis tests were two-tailed and data are shown as mean +/- sem.

DATA AVAILABILITY

RNAseq data analyzed in Supplementary Fig. 1 were generated in reference 22 and are available on FigShare at the following link: https://figshare.com/projects/Continuous_and_discrete_neuron_types_of_the_adult_murine_striatum/69080. All other data in the paper are available on Zenodo: 10.5281/zenodo.18332283.

CODE AVAILABILITY

Code used in this study is available on Github: https://github.com/dcardozop/CardozoPinto_Guo_2026_NatCommun. It is linked to the data repository on Zenodo at the doi: 10.5281/zenodo.18332283.

REFERENCES

1. Costa, K. M. & Schoenbaum, G. Dopamine. *Current Biology* **32**, R817–R824 (2022).
2. Boureau, Y.-L. & Dayan, P. Opponency Revisited: Competition and Cooperation Between Dopamine and Serotonin. *Neuropsychopharmacology* **36**, 74–97 (2011).
3. Daw, N. D., Kakade, S. & Dayan, P. Opponent interactions between serotonin and dopamine. *Neural Networks* **15**, 603–616 (2002).
4. Cools, R., Nakamura, K. & Daw, N. D. Serotonin and Dopamine: Unifying Affective, Activational, and Decision Functions. *Neuropsychopharmacology 2011 36:1* **36**, 98–113 (2010).
5. Soubrié, P. Reconciling the role of central serotonin neurons in human and animal behavior. *Behavioral and Brain Sciences* **9**, 319–335 (1986).
6. Deakin, J. F. W. & Graeff, F. G. 5-HT and mechanisms of defence. *Journal of Psychopharmacology* **5**, 305–315 (1991).
7. Mkrtchian, A. *et al.* Differential Associations of Dopamine and Serotonin With Reward and Punishment Processes in Humans. *JAMA Psychiatry* **82**, 818 (2025).
8. Wee, S. & Woolverton, W. L. Self-administration of mixtures of fenfluramine and amphetamine by rhesus monkeys. *Pharmacol Biochem Behav* **84**, 337–343 (2006).
9. Wee, S. *et al.* Relationship between the serotonergic activity and reinforcing effects of a series of amphetamine analogs. *Journal of Pharmacology and Experimental Therapeutics* **313**, 848–854 (2005).
10. Carroll, M. E., Lac, S. T., Asencio, M. & Kragh, R. Fluoxetine reduces intravenous cocaine self-administration in rats. *Pharmacol Biochem Behav* **35**, 237–244 (1990).
11. Howell, L. L. & Byrd, L. D. Serotonergic modulation of the behavioral effects of cocaine in the squirrel monkey. *J Pharmacol Exp Ther* **275**, 1551–1559 (1995).
12. Miyazaki, K. W. *et al.* Optogenetic activation of dorsal raphe serotonin neurons enhances patience for future rewards. *Current Biology* **24**, 2033–2040 (2014).
13. Miyazaki, K. *et al.* Reward probability and timing uncertainty alter the effect of dorsal raphe serotonin neurons on patience. *Nat Commun* **9**, (2018).
14. Miyazaki, K., Miyazaki, K. W. & Doya, K. Activation of dorsal raphe serotonin neurons underlies waiting for delayed rewards. *Journal of Neuroscience* **31**, (2011).

15. Miyazaki, K. W., Miyazaki, K. & Doya, K. Activation of dorsal raphe serotonin neurons is necessary for waiting for delayed rewards. *Journal of Neuroscience* **32**, (2012).

16. Miyazaki, K. *et al.* Serotonergic projections to the orbitofrontal and medial prefrontal cortices differentially modulate waiting for future rewards. *Sci Adv* **6**, (2020).

17. Cardozo Pinto, D. F. *et al.* Opponent control of reinforcement by striatal dopamine and serotonin. *Nature* **639**, 143–152 (2025).

18. Surmeier, D. J., Ding, J., Day, M., Wang, Z. & Shen, W. D1 and D2 dopamine-receptor modulation of striatal glutamatergic signaling in striatal medium spiny neurons. *Trends Neurosci* **30**, 228–235 (2007).

19. Gerfen, C. R. & Surmeier, D. J. Modulation of striatal projection systems by dopamine. *Annu Rev Neurosci* **34**, 441–66 (2011).

20. De Filippo, R. & Schmitz, D. Transcriptomic mapping of the 5-HT receptor landscape. *Patterns* 101048 (2024) doi:10.1016/j.patter.2024.101048.

21. Radja, F. *et al.* Autoradiography of serotonin receptor subtypes in the central nervous system. *Neurochem Int* **18**, 1–15 (1991).

22. Stanley, G., Gokce, O., Malenka, R. C., Südhof, T. C. & Quake, S. R. Continuous and Discrete Neuron Types of the Adult Murine Striatum. *Neuron* **105**, 688-699.e8 (2020).

23. Gokce, O. *et al.* Cellular Taxonomy of the Mouse Striatum as Revealed by Single-Cell RNA-Seq. *Cell Rep* **16**, 1126–1137 (2016).

24. Tran, M. N. *et al.* Single-nucleus transcriptome analysis reveals cell-type-specific molecular signatures across reward circuitry in the human brain. *Neuron* **109**, 3088-3103.e5 (2021).

25. Azmitia, E. C. & Segal, M. An autoradiographic analysis of the differential ascending projections of the dorsal and median raphe nuclei in the rat. *Journal of Comparative Neurology* **179**, 641–667 (1978).

26. Soghomonian, J. J., Doucet, G. & Descarries, L. Serotonin innervation in adult rat neostriatum. I. Quantified regional distribution. *Brain Res* **425**, 85–100 (1987).

27. Beal, M. F. & Martin, J. B. Topographical dopamine and serotonin distribution and turnover in rat striatum. *Brain Res* **358**, 10–15 (1985).

28. Steinbusch, H. W. M. Distribution of serotonin-immunoreactivity in the central nervous system of the rat—Cell bodies and terminals. *Neuroscience* **6**, 557–618 (1981).

29. Parent, M., Wallman, M. J., Gagnon, D. & Parent, A. Serotonin innervation of basal ganglia in monkeys and humans. *J Chem Neuroanat* **41**, 256–265 (2011).

30. Lavoie, B. & Parent, A. Immunohistochemical study of the serotoninergic innervation of the basal ganglia in the squirrel monkey. *Journal of Comparative Neurology* **299**, 1–16 (1990).

31. Horn, R. & Marty, A. Muscarinic activation of ionic currents measured by a new whole-cell recording method. *Journal of General Physiology* **92**, 145–159 (1988).

32. Lahiri, A. K. & Bevan, M. D. Dopaminergic Transmission Rapidly and Persistently Enhances Excitability of D1 Receptor-Expressing Striatal Projection Neurons. *Neuron* **106**, 277-290.e6 (2020).

33. Hunker, A. C. *et al.* Conditional Single Vector CRISPR/SaCas9 Viruses for Efficient Mutagenesis in the Adult Mouse Nervous System. *Cell Rep* **30**, (2020).

34. Andrews, C. & Lucki, I. Effects of cocaine on extracellular dopamine and serotonin levels in the nucleus accumbens. *Psychopharmacology (Berl)* **155**, 221–229 (2001).

35. Parsons, L. H. & Justice, J. B. Serotonin and Dopamine Sensitization in the Nucleus Accumbens, Ventral Tegmental Area, and Dorsal Raphe Nucleus Following Repeated Cocaine Administration. *J Neurochem* **61**, 1611–1619 (1993).

36. Bachtell, R. K., Whisler, K., Karanian, D. & Self, D. W. Effects of intranucleus accumbens shell administration of dopamine agonists and antagonists on cocaine-taking and cocaine-seeking behaviors in the rat. *Psychopharmacology (Berl)* **183**, 41–53 (2005).

37. Chen, R. *et al.* Abolished cocaine reward in mice with a cocaine-insensitive dopamine transporter. *Proceedings of the National Academy of Sciences* **103**, 9333–9338 (2006).

38. Lobo, M. K. *et al.* Cell Type–Specific Loss of BDNF Signaling Mimics Optogenetic Control of Cocaine Reward. *Science (1979)* **330**, 385–390 (2010).

39. Heinsbroek, J. A. *et al.* Loss of Plasticity in the D2-Accumbens Pallidal Pathway Promotes Cocaine Seeking. *The Journal of Neuroscience* **37**, 757–767 (2017).

40. Bock, R. *et al.* Strengthening the accumbal indirect pathway promotes resilience to compulsive cocaine use. *Nat Neurosci* **16**, 632–638 (2013).

41. North, R. A. & Uchimura, N. 5-Hydroxytryptamine acts at 5-HT2 receptors to decrease potassium conductance in rat nucleus accumbens neurones. *J Physiol* **417**, 1–12 (1989).

42. Stefani, A., Surmeier, D. J. & Kitai, S. T. Serotonin enhances excitability in neostriatal neurons by reducing voltage-dependent potassium currents. *Brain Res* **529**, 354–357 (1990).

43. Cunningham, K. A. *et al*. Selective serotonin 5-HT2C receptor activation suppresses the reinforcing efficacy of cocaine and sucrose but differentially affects the incentive-salience value of cocaine- vs. sucrose-associated cues. *Neuropharmacology* **61**, 513–523 (2011).

44. Salinsky, L. M. *et al*. The psychedelic (−)-2,5-dimethoxy-4-iodoamphetamine [(−)-DOI] demonstrates efficacy in reducing cocaine reward and motivation in male rats. *Psychopharmacology (Berl)* **242**, 1833–1844 (2025).

45. Higgins, G. A. & Fletcher, P. J. Therapeutic Potential of 5-HT2C Receptor Agonists for Addictive Disorders. *ACS Chem Neurosci* **6**, 1071–1088 (2015).

46. Higgins, G. A. & Fletcher, P. J. Serotonin and drug reward: focus on 5-HT2C receptors. *Eur J Pharmacol* **480**, 151–162 (2003).

47. Howell, L. L. & Cunningham, K. A. Serotonin 5-ht2 receptor interactions with dopamine function: Implications for therapeutics in cocaine use disorder. *Pharmacol Rev* **67**, 176–197 (2015).

48. Li, Y. *et al*. Synaptic mechanism underlying serotonin modulation of transition to cocaine addiction. *Science (1979)* **373**, (2021).

49. Pelloux, Y., Dilleen, R., Economidou, D., Theobald, D. & Everitt, B. J. Reduced forebrain serotonin transmission is causally involved in the development of compulsive cocaine seeking in rats. *Neuropsychopharmacology* **37**, 2505–2514 (2012).

50. Rocha, B. A. *et al*. Enhanced locomotor, reinforcing, and neurochemical effects of cocaine in serotonin 5-hydroxytryptamine 2C receptor mutant mice. *Journal of Neuroscience* **22**, (2002).

51. Grottick, A. J., Corrigall, W. A. & Higgins, G. A. Activation of 5-HT2C receptors reduces the locomotor and rewarding effects of nicotine. *Psychopharmacology (Berl)* **157**, (2001).

52. Tomkins, D. M. *et al.* An investigation of the role of 5-HT2C receptors in modifying ethanol self-administration behaviour. *Pharmacol Biochem Behav* **71**, (2002).

53. Cameron, L. P. *et al.* A non-hallucinogenic psychedelic analogue with therapeutic potential. *Nature 2020 589:7842* **589**, 474–479 (2020).

54. Pomrenze, M. B. *et al.* 5-HT2C receptors in the nucleus accumbens constrain the rewarding effects of MDMA. *Mol Psychiatry* **30**, 5405–5416 (2025).

55. Bonilla, J. *et al.* The psychedelic drug DOI reduces heroin motivation by targeting 5-HT2A receptors in a heroin and alcohol co-use model. *Neuropharmacology* **261**, 110163 (2024).

56. Zhang, G. *et al.* Activation of serotonin 5-HT2C receptor suppresses behavioral sensitization and naloxone-precipitated withdrawal symptoms in morphine-dependent mice. *Neuropharmacology* **101**, (2016).

57. Cameron, L. P. *et al.* Beyond the 5-HT2A Receptor: Classic and Nonclassic Targets in Psychedelic Drug Action. *Journal of Neuroscience* **43**, (2023).

58. Winkelman, M. Psychedelics as medicines for substance abuse rehabilitation: Evaluating treatments with LSD, peyote, ibogaine and Ayahuasca. *Curr Drug Abuse Rev* **7**, (2014).

59. Morgan, C., McAndrew, A., Stevens, T., Nutt, D. & Lawn, W. Tripping up addiction: the use of psychedelic drugs in the treatment of problematic drug and alcohol use. *Curr Opin Behav Sci* **13**, 71–76 (2017).

60. González-Maeso, J. *et al.* Hallucinogens Recruit Specific Cortical 5-HT2A Receptor-Mediated Signaling Pathways to Affect Behavior. *Neuron* **53**, (2007).

61. Kwan, A. C., Olson, D. E., Preller, K. H. & Roth, B. L. The neural basis of psychedelic action. *Nat Neurosci* **25**, 1407–1419 (2022).

62. Mathur, B. N., Capik, N. A., Alvarez, V. A. & Lovinger, D. M. Serotonin Induces Long-Term Depression at Corticostriatal Synapses. *Journal of Neuroscience* **31**, 7402–7411 (2011).

63. Reynolds, J. N. J. & Wickens, J. R. Substantia nigra dopamine regulates synaptic plasticity and membrane potential fluctuations in the rat neostriatum, in vivo. *Neuroscience* **99**, 199–203 (2000).

64. Reynolds, J. N. J. & Wickens, J. R. Dopamine-dependent plasticity of corticostriatal synapses. *Neural Networks* **15**, 507–521 (2002).

65. Cavaccini, A. *et al.* Serotonergic Signaling Controls Input-Specific Synaptic Plasticity at Striatal Circuits. *Neuron* **98**, 801-816.e7 (2018).

66. Christoffel, D. J. *et al.* Selective filtering of excitatory inputs to nucleus accumbens by dopamine and serotonin. *Proc Natl Acad Sci U S A* **118**, (2021).

67. Dobbs, L. K. K. *et al.* Dopamine Regulation of Lateral Inhibition between Striatal Neurons Gates the Stimulant Actions of Cocaine. *Neuron* **90**, 1100–1113 (2016).

68. Burke, D. A. & Alvarez, V. A. Serotonin receptors contribute to dopamine depression of lateral inhibition in the nucleus accumbens. *Cell Rep* **39**, (2022).

69. Pommer, S., Akamine, Y., Schiffmann, S. N., de Kerchove d'Exaerde, A. & Wickens, J. R. The effect of serotonin receptor 5-HT1B on lateral inhibition between spiny projection neurons in the mouse striatum. *Journal of Neuroscience* **41**, 7831–7847 (2021).

70. Virk, M. S. *et al.* Opposing roles for serotonin in cholinergic neurons of the ventral and dorsal striatum. *Proc Natl Acad Sci U S A* **113**, 734–739 (2016).

71. Chantranupong, L. *et al.* Dopamine and glutamate regulate striatal acetylcholine in decision-making. *Nature 2023 621:7979* **621**, 577–585 (2023).

72. Blomeley, C. & Bracci, E. Excitatory effects of serotonin on rat striatal cholinergic interneurones. *J Physiol* **569**, 715–721 (2005).

73. Blomeley, C. P. & Bracci, E. Serotonin excites fast-spiking interneurons in the striatum. *European Journal of Neuroscience* **29**, 1604–1614 (2009).

74. Cains, S., Blomeley, C. P. & Bracci, E. Serotonin inhibits low-threshold spike interneurons in the striatum. *J Physiol* **590**, 2241–2252 (2012).

75. Bonsi, P. *et al.* Endogenous Serotonin Excites Striatal Cholinergic Interneurons via the Activation of 5-HT 2C, 5-HT6, and 5-HT7 Serotonin Receptors: Implications for Extrapyramidal Side Effects of Serotonin Reuptake Inhibitors. *Neuropsychopharmacology* **32**, 1840–1854 (2007).

76. Vizi, E. S., Hársing, L. G. & Zsilla, G. Evidence of the modulatory role of serotonin in acetylcholine release from striatal interneurons. *Brain Res* **212**, 89–99 (1981).

77. Alcantara, A. A., Chen, V., Herring, B. E., Mendenhall, J. M. & Berlanga, M. L. Localization of dopamine D2 receptors on cholinergic interneurons of the dorsal striatum and nucleus accumbens of the rat. *Brain Res* **986**, 22–29 (2003).

78. Xu, S., Das, G., Hueske, E. & Tonegawa, S. Dorsal Raphe Serotonergic Neurons Control Intertemporal Choice under Trade-off. *Current Biology* **27**, 3111-3119.e3 (2017).

79. Eshel, N. *et al*. Striatal dopamine integrates cost, benefit, and motivation. *Neuron* **112**, 500-514.e5 (2024).

80. Dölen, G., Darvishzadeh, A., Huang, K. W. & Malenka, R. C. Social reward requires coordinated activity of nucleus accumbens oxytocin and serotonin. *Nature* **501**, 179–184 (2013).

81. Walsh, J. J. *et al*. 5-HT release in nucleus accumbens rescues social deficits in mouse autism model. *Nature* **560**, 589–594 (2018).

82. Gunaydin, L. A. *et al*. Natural neural projection dynamics underlying social behavior. *Cell* **157**, 1535–1551 (2014).

83. Willmore, L., Cameron, C., Yang, J., Witten, I. B. & Falkner, A. L. Behavioural and dopaminergic signatures of resilience. *Nature* **611**, 124–132 (2022).

84. Dai, B. *et al*. Responses and functions of dopamine in nucleus accumbens core during social behaviors. *Cell Rep* **40**, 111246 (2022).

85. Martin, H., Choi, J. E., Rodrigues, A. R. & Eshel, N. Review: Dopamine, Serotonin, and the Translational Neuroscience of Aggression in Autism Spectrum Disorder. *JAACAP Open* **3**, 29–41 (2025).

86. Pomrenze, M. B. *et al*. Modulation of 5-HT release by dynorphin mediates social deficits during opioid withdrawal. *Neuron* **110**, (2022).

87. Li, C. H. & Tam, P. K. S. An iterative algorithm for minimum cross entropy thresholding. *Pattern Recognit Lett* **19**, 771–776 (1998).

88. Tsai, W. H. Moment-preserving thresolding: A new approach. *Comput Vis Graph Image Process* **29**, 377–393 (1985).

89. Paxinos, George. & Franklin, K. B. J. . *The Mouse Brain in Stereotaxic Coordinates*. (Academic Press, 2001).

90. Perkins, K. L. Cell-attached voltage-clamp and current-clamp recording and stimulation techniques in brain slices. *J Neurosci Methods* **154**, 1–18 (2006).

91. Cardozo Pinto, D. F. et al. Characterization of transgenic mouse models targeting neuromodulatory systems reveals organizational principles of the dorsal raphe. *Nat. Commun.* **10**, 4633 (2019).

ACKNOWLEDGMENTS

We thank members of the Malenka lab, STAAR lab, and Austen B. Casey for discussions, the Stanford Gene Vector and Virus Core for reagents, and Selena Schattauer and Ella Kirwan for assistance in production of AAV CRISPR constructs. This work was supported by philanthropic funds donated to the Nancy Pritzker Laboratory at Stanford University, an NSF Graduate Research Fellowship (D.F.C.P.), an HHMI Gilliam Fellowship for Advanced Study (D.F.C.P. and R.C.M.), a Stanford Vice Provost for Undergraduate Education Major Grant (M.Y.G.), a Brain & Behavior Research Foundation Young Investigator Grant (N.E.), a Burroughs Wellcome Fund Career Award for Medical Scientists (N.E.), a Stanford NeuroChoice Initiative Pilot Award (N.E.), a Simons Foundation Bridge to Independence Award (N.E.), a grant from the Stanford Wu Tsai Neurosciences Institute (R.C.M.), a grant from the UCSF Dolby Family Center for Mood Disorders (R.C.M.), and NIH grants K99DA056573 (M.B.P.), K08MH123791 (N.E.), R01MH138645 (N.E.), P30DA048736 (L.S.Z.), and P50DA042012 (R.C.M.).

AUTHOR CONTRIBUTIONS

D.F.C.P., N.E., and R.C.M. conceived the study and designed the experiments. M.Y.G collected fluorescence *in situ* hybridization and fiber photometry data. M.Y.G and M.X.L collected cfos data. W.M. collected electrophysiology data. M.B.P. collected CPP data. D.F.C.P. collected axon bouton tracing data. L.S.Z. provided the CRISPR viruses. N.E. and R.C.M. provided funding and key resources. D.F.C.P. analyzed the data and made the figures with assistance from M.Y.G., M.B.P., and W.M. The manuscript was written by D.F.C.P., N.E., and R.C.M. and edited by all authors.

COMPETING INTERESTS

N.E. is a consultant for Boehringer Ingelheim. R.C.M. is an advisor to Bayshore Global Management and is on the scientific advisory boards of MapLight Therapeutics, Definium Therapeutics, and Aelis Farma. The remaining authors declare no competing interests.

ADDITIONAL INFORMATION

Supplementary information is available for this paper.

Correspondence and requests for materials should be addressed to Daniel F. Cardozo Pinto (dcardozopinto@fas.harvard.edu), Neir Eshel (neshel@stanford.edu) and Robert C. Malenka (malenka@stanford.edu).

FIGURE LEGENDS

Fig. 1: Differential 5HT receptor expression profiles between pD1- and pD2-MSNs

a, Left, fluorescence *in situ* hybridization labeling of *Drd1a, Drd2, and Htr1b* in the striatum. Center, reconstruction of the relative expression of *Htr1b* in the striatum. Each pMSN is represented by a dot, dots are colored by cell-type, and the size and opacity of each dot scales with the relative expression of *Htr1b* in that cell. Right, quantification of the relative expression of *Htr1b* across striatal subregions and cell-types (n=9 mice). **b,** Same as **a**, but for *Htr1d* (n=9 mice). **c,** Same as **a**, but for *Htr1f* (n=8 mice). **d,** Same as **a**, but for *Htr2a* (n=9 mice). **e,** Same as **a**, but for *Htr2c* (n=9 mice). **f,** Same as **a**, but for *Htr4* (n=9 mice). **g,** Same as **a**, but for *Htr6* (n=8 mice). **h,** Same as **a**, but for *Htr7* (n=8 mice). **i-j,** Schematics summarizing relative 5HT receptor expression (**i**) and 5HT axon density (**j**) across striatal subregions. **k,** Cell-type preference analysis for 5HT receptor expression in the NAc^{medSh} (n=9 mice: *Htr1b*, *Htr1d*, *Htr2a*, *Htr2c*, *Htr4*; n=8 mice: *Htr1f*, *Htr6*, *Htr7*). For this and all subsequent figures, data are shown as mean ± s.e.m., significance is denoted as *P < 0.05, **P < 0.01, ***P < 0.001, ****P < 0.0001, significance tests were two-tailed, and statistics are shown in Supplementary Table 1. Credits: mouse brain schematic, adapted from ref.[91] (https://creativecommons.org/licenses/by/4.0/).

Fig. 2: DA and 5HT differentially regulate activity of D1- and D2-MSNs

a, Genetic strategy for cell-attached recordings from D1- and D2-MSNs. **b,** Top, schematic of experimental design for cell-attached recordings. Bottom, example trace showing addition of Ba^{2+} and 4-AP induces spontaneous activity in an MSN. **c,** Spontaneous activity induced by Ba^{2+} and 4-AP did not differ between D1- and D2- MSNs (D1-MSNs: n=32 cells from 10 mice; D2-MSNs: 36 cells from 13 mice). **d-e,** Example traces depicting D1-MSNs before (top) and after (bottom) addition of DA (**d**), and corresponding quantification of action potential frequency (**e**, n=12 cells from 4 mice). **f-g**, same as **d-e** but for D2-MSNs (n=14 cells from 4 mice). **h-i,** Example traces depicting D1-MSNs before (top) and after (bottom) addition of 5HT (**h**), and corresponding quantification of action potential frequency (**i**, n= 20 cells from 6 mice). **j-k**, same

as **h-i** but for D2-MSNs (n=22 cells from 9 mice). **l-m**, Relative changes (**l,** difference; **m**, ratio) in D1- and D2-MSN activity following application of DA or 5HT (D1-DA, n= 12 cells from 4 mice; D2-DA, n= 14 cells from 4 mice; D1-5HT, n=20 cells from 6 mice; D2-5HT n=22 cells from 9 mice). **n**, Top, schematic of experimental design for cell-attached recordings with 5HT2 receptor antagonists. Bottom, example traces showing D2-MSN activity before (left) and after (right) application of 5HT in the presence of 5HT2 receptor antagonists. **o**, Quantification of action potential frequency for the experiment described in **n** (n= 18 cells from 6 mice). **p**, Experimental strategy for intra-NAc drug infusion experiments followed by cfos immunohistochemistry in *Drd1a-TdTom;Drd2-eGFP* double transgenic mice. **q**, Example confocal images showing cfos expression in saline- and escitalopram- (2.5 ug) treated mice (6-8 sections imaged from each of n=3 and n=5 mice in SAL and ESC groups, respectively). **r-t**, Sum (**r**), difference (**s**), and percentage (**t**) of D1- and D2-MSNs that were cfos positive in saline- and escitalopram- treated mice (SAL, n=3 mice; ESC, n=5 mice). In **d**,**f**,**h**,**i**,and **n** tick marks indicate where calibration pulse artifacts were manually removed, and in **d**,**f**,**h**, and **i** arrows indicate corresponding locations on the example traces (left) and their magnified insets (right). Credits: mouse, adapted from NIH BioArt (https://bioart.niaid.nih.gov/bioart/279); mouse brain schematic, adapted from ref.[91] (https://creativecommons.org/licenses/by/4.0/).

Fig. 3: 5HTergic modulation of D2-MSNs constrains DA's reinforcing effects

a, Viral strategy for cell-type specific mutagenesis of *Htr2c* or *Rosa26* in D1- or D2-MSNs. **b**, Design of cocaine CPP experiment. **c**, Distance traveled during each cocaine conditioning session for D1-sgRosa and D1-sgHtr2c mice. **d**, Distance traveled during the last cocaine conditioning session normalized to distance traveled during the first saline conditioning session for D1-sgRosa and D1-sgHtr2c mice. **e-f**, Cocaine CPP scores for D1-sgRosa and D1-sgHtr2c mice. For **c-f**, n=8 D1-sgRosa mice, n=10 D1-sgHtr2c mice. **g**, Same as **c** but for D2-sgRosa and D2-sgHtr2c mice. **h**, Same as **d** but for D2-sgRosa and D2-sgHtr2c mice. **i-j**, Same as **e-f** but for D2-sgRosa and D2-sgHtr2c mice. For **g-j**, n=8 D2-sgRosa mice, and n=10 D2-sgHtr2c mice. **k-l**, comparison of cocaine CPP scores between D1-sgHtr2c, D2-sgHtr2c, and sgRosa (combined D1-sgRosa and D2-sgRosa) groups. **m-n**, Correlation analysis between measures of cocaine's locomotor and rewarding effects for mice in the D1-sgHtr2c, D2-sgHtr2c, and sgRosa groups. For **k-n**, n=16 sgRosa mice, n=10 D1-sgHtr2c mice, n=10 D2-sgHtr2c mice. Credits: mouse brain schematic, adapted from ref.[91] (https://creativecommons.org/licenses/by/4.0/).

Editor's summary:

It remains unclear how opponent serotonin and dopamine signals regulate striatal activity to exert opposing effects on behavior. This study reveals how the complement of serotonin and dopamine receptors expressed by cells in the striatum enable the two neuromodulators to exert opposing functions during reward learning.

Peer review information: *Nature Communications* thanks the anonymous reviewer(s) for their contribution to the peer review of this work. A peer review file is available.

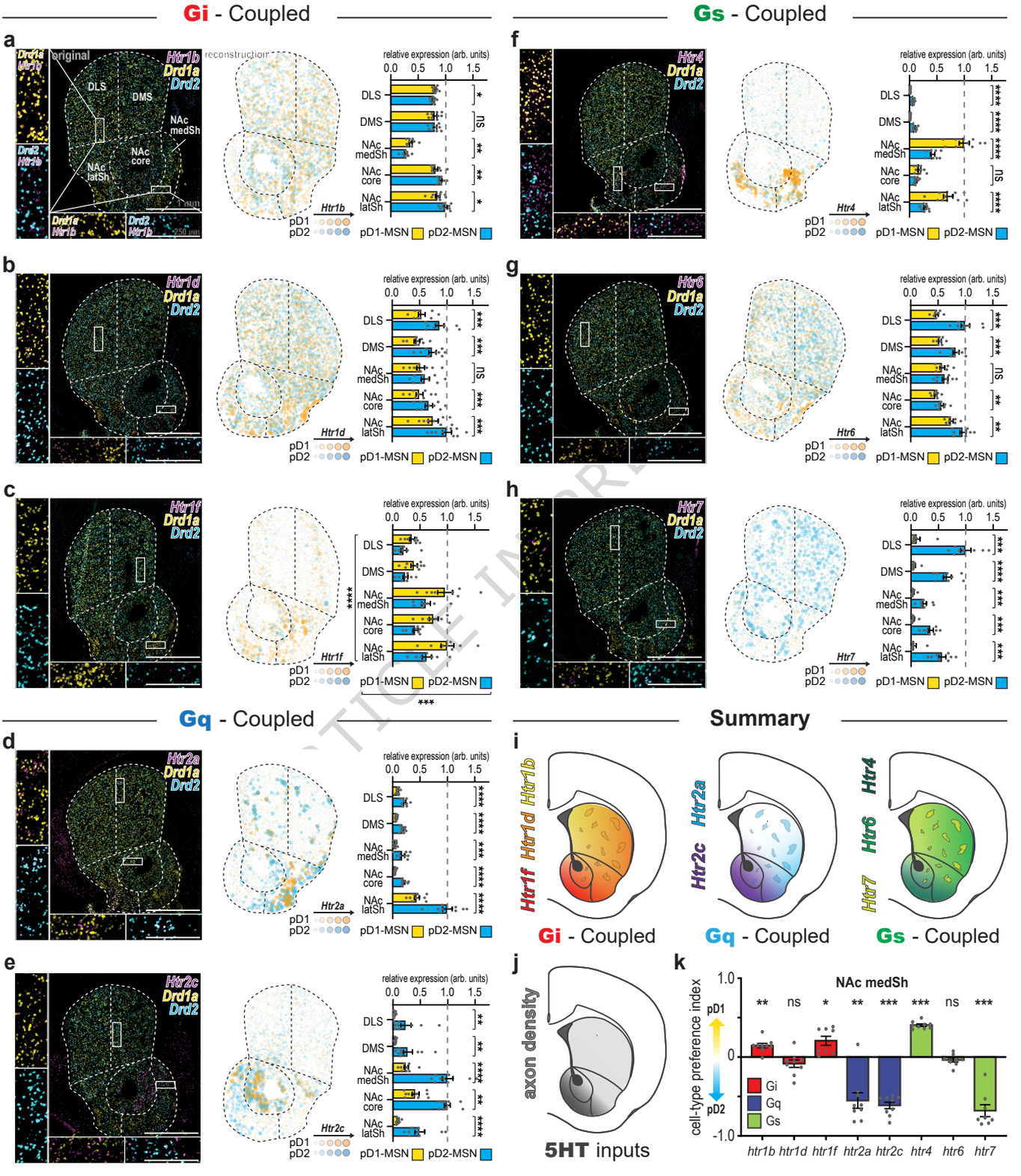
Gi - Coupled
Gs - Coupled
Gq - Coupled
Summary
a
b
c
d
e
f
g
h
i
j
k
original
reconstruction
DLS
DMS
NAc medSh
NAc core
NAc latSh
Drd1a Htr1b
Drd2 Htr1b
Htr1b Drd1a Drd2
Htr1d Drd1a Drd2
Htr1f Drd1a Drd2
Htr2a Drd1a Drd2
Htr2c Drd1a Drd2
Htr4 Drd1a Drd2
Htr6 Drd1a Drd2
Htr7 Drd1a Drd2
relative expression (arb. units)
0.0 0.5 1.0 1.5
pD1
pD2
pD1-MSN
pD2-MSN
axon density
5HT inputs
cell-type preference index
NAc medSh
pD1
pD2
Gi
Gq
Gs
htr1b htr1d htr1f htr2a htr2c htr4 htr6 htr7

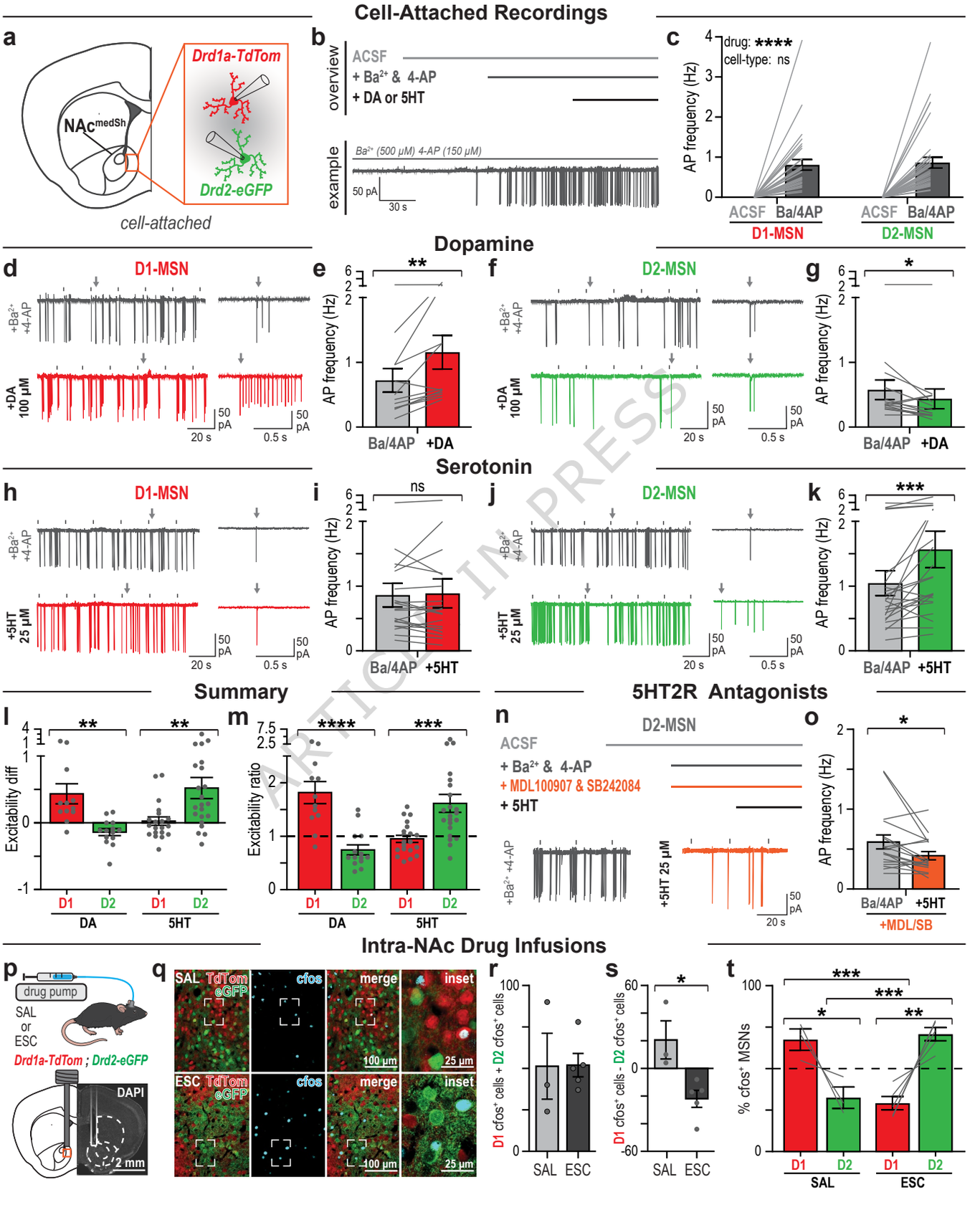

Overview

Htr2c loss-of-function in D1-MSNs

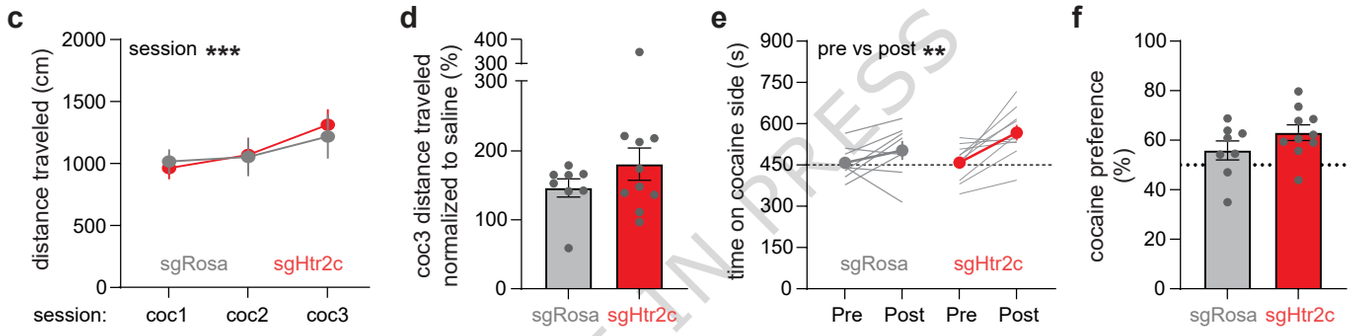

Htr2c loss-of-function in D2-MSNs

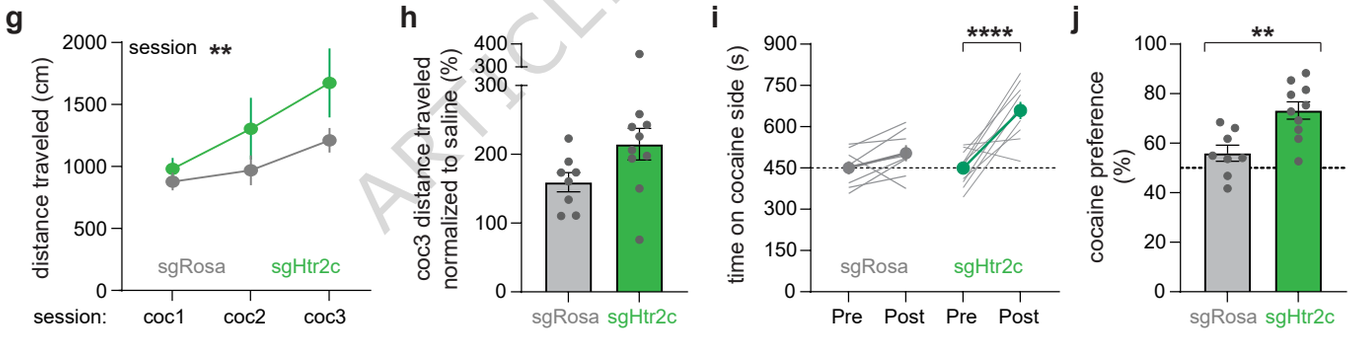

Summary